Journal of Fluids and Structures 103 (2021) 103282

Contents lists available at ScienceDirect

Journal of Fluids and Structures

journal homepage: www.elsevier.com/locate/jfs

Experimental study on characteristics of vortex-induced vibration of a twin-box girder and damping effects

Buchen Wu [c,d,e], Shujin Laima [a,b,c,*]

[a] Key Lab of Smart Prevention and Mitigation for Civil Infrastructures, Ministry of Industry and Information Technology, Harbin, Heilongjiang 150090, China
[b] Key Lab of Structures Dynamic Behavior and Control of the Ministry of Education, Harbin Institute of Technology, Harbin, 150090, China
[c] School of Civil Engineering, Harbin Institute of Technology, Harbin, Heilongjiang 150090, China
[d] Department of Mechanical Engineering, National University of Singapore, 117575, Singapore
[e] Department of Mechanics and Aerospace Engineering, Southern University of Science and Technology, Shenzhen, Guangdong 518055, China

ARTICLE INFO

Article history:
Received 19 August 2020
Received in revised form 1 February 2021
Accepted 1 April 2021
Available online 16 April 2021

Keywords:
Vortex-induced vibration
Twin-box girder
Flow pattern
Aerodynamic force
Damping effect

ABSTRACT

To investigate the characteristics of vortex-induced vibration (VIV) of the twin-box girder, we carried out the VIV wind tunnel tests. The VIV of the twin-box girder occurs in the range of $4.680 \leq U_r \leq 6.113$, with the maximum dimensionless VIV displacement RMS(y)/D=0.03308 at reduced velocity at $U_r = 5.949$. It is interesting that the VIV suddenly disappears at $U_r = 6.276$ at the loading stage, and the large amplitude VIV does not occur at the unloading stage, which indicates that the vibration trajectory with the variation of reduced wind velocity shows significant asymmetry characteristic. In the lock-in region, as the aerodynamic lift force increases, both the phase lag and the VIV displacement show an increasing tendency with the reduced velocity. Flow visualization results show that strong alternately shedding vortex generates around the gap during the VIV. Under the effects of the vortex in the gap, the size of the separation bubble increases with the increase of vibration amplitude, and the wake width becomes wider. As the damping ratio increases, the amplitude of VIV displacement shows a decreasing tendency, the lock-in region becomes narrower and the reduced velocity corresponding to the max VIV displacement decreases. Moreover, the maximum RMS displacement of vertical VIV decays exponentially as the damping ratio increases.

1. Introduction

Under the condition of large-scale construction of long-span bridges, the safety of bridges structures is more frequently concerned. In particular, the effect of wind-induced vibration (vortex-induced vibration (VIV) and flutter) significantly impacts on the stability of the bridge structures. Streamlined twin-box girder is a popular section configuration adopted in the long-span bridges, for example, the Xihoumen suspension bridge with the main span of 1650 m, the Gwangyang suspension bridge with the main span of 1545 m, and the Stonecutters' cable-stayed Bridge with the main span of 1018 m. Although the twin-separated box girder has great aerodynamic advantages in flutter stability (Ge et al., 2011), the

* Corresponding author at: Key Lab of Smart Prevention and Mitigation for Civil Infrastructures, Ministry of Industry and Information Technology, Harbin, Heilongjiang 150090, China.
E-mail address: laimashujin@hit.edu.cn (S. Laima).

https://doi.org/10.1016/j.jfluidstructs.2021.103282
0889-9746/

complex section configuration, especially the gap between upstream and downstream parallel box girders, produces more complicated flow structures around twin-box girders.

It is generally acknowledged that the VIV is caused by the vortex shedding frequency close to the natural frequency of the solid body, so the probability of the occurrence of VIV is quite high in natural environment. Although the amplitude of vertical displacement of VIV is limit, which differs considerably from the flutter phenomenon and cannot devastate the bridges, it might cause discomfort for drivers and can reduce the service life of the bridge structures induced by long-term fatigue damage at low flow velocity. In the last decades, the VIV of long-span bridges is more frequently observed (Larsen et al., 2000; Frandsen, 2001; Fujino and Yoshida, 2002; Li et al., 2011, 2014). Hence, it is necessary to conduct the investigation concerned about the VIV characteristics of the long-span bridge with a twin-box girder, which is frequently used to link mainland to islands with important strategic and economic values because of its special geographical position. There are many studies about VIVs of bluff body (e.g. circular cylinder; square cylinder) by wind tunnel tests or numerically simulations, and the mechanisms of VIVs of the bluff body have been deeply investigated. The phase jump between two amplitude branches, an important phenomenon in the VIV of the cylinder, is caused by the vortex-shedding mode switching and the vortex-shedding pattern change from 2S mode to 2P mode indicates that phase jump from the upper branch to the lower one (Feng, 1968; Williamson and Roshko, 1988; Brika and Laneville, 1993). Klamo et al. (2005) confirmed that the maximum vertical displacement of the VIV of circular cylinders is closely related to the damping ratios, which demonstrates that the damping ratio is a crucial factor in controlling the VIV behaviors.

Owing to the different aerodynamic configurations, the mechanisms of VIVs of the bare cylinder cannot directly apply to streamlined box girders. Diana et al. (2006) experimentally studied the effect of vortex-shedding on the multiple box deck of Messina Strait Bridge, and proposed a numerical model to calculate the vortex shedding forces. Larsen et al. (2008) studied the guide vane countermeasure to suppress VIV of a twin-separated box girder at various Reynolds numbers. They pointed out that the displacement thickness should be about 10% of the guide vane offset, allowing a sufficient flow rate to promote guide vane's efficiency. Li and Ge (2008) investigated the response of VIV of a twin-box girder with different size guide vanes at various locations. And the experimental results demonstrate that the size and location of guide vanes are a significant factor for the response of VIV of a twin-box girder. Yang et al. (2016) studied the VIV characteristics of a box girder with various slot ratios and evaluate the efficiency of four countermeasures of surprising the VIV of twin-box girder, including increasing structural damping ratio, installing grid plate, wind barriers and guide vanes. The results show that increasing structural damping could reduce the VIV response, while installing guide vanes has adverse effect. Grid plate and wind barriers can suppress the vertical VIV. Ma et al. (2018) investigated the responses of the VIV motion of a twin-box girder in wind tunnel tests. The results indicated that the grid plates that could eliminate the generation of the large-scale vortex could suppress the VIV of a twin-box girder efficiently, and the effect of grid plates is dependent on the design parameters. Li et al. (2018) numerically investigated the suppression effect of central grids on the VIVs of twin-box girders using delayed detached eddy simulation (DDES). The results shows that the central grids could significantly suppress VIVs of the twin-box girder. Zhou et al. (2018) evaluated the effectiveness of vertical central stabilizer (VCS) on vortex-induced vibration of a twin-box girder. And the results showed that the vertical displacement of VIV of a twin-box girder with higher upward VCS (UVCS) and downward VCS (DVCS) increases significantly. The characteristics of VIV response of the twin-box girder, and the vortex behaviors during the process of the VIV, and the effects of attachments, gap width, and Reynolds number on the VIV of the twin-box girder are comprehensively evaluated (Li et al., 2011, 2014; Laima et al., 2013; Laima and Li, 2015; Laima et al., 2018).

The characteristics of aerodynamic forces, such as force amplitude, phase referring to displacement, aerodynamic damping and stiffness forces, are important factors to understand the process of fluid–structure interaction during VIV. However, it is not easy to measure the aerodynamic forces unless the force signal and displacement signal have high synchronicity and the damping of the measured section between the force sensors can be accuracy obtained or omitted (Gao and Zhu, 2015; Gao et al., 2018). An alternative method is that we can identify the aerodynamic forces based on measured dynamic response (displacement or acceleration). For the study, the latter method is adopted. As well known, structural damping is one of very important factor to affect the VIV behaviors of bridge deck. For the long-span bridge, the VIV response and lock-in range are very sensitive to the damping. Therefore, the characteristics of aerodynamic forces and damping effects are two curious concerns to study the VIV of bridge deck. However, the characteristics of aerodynamic forces during the VIV and the damping effects on the VIV development are not yet revealed in our previous articles. Therefore, the main objective of the study is to investigate the aerodynamic characteristics of VIVs of a twin-box girder and the damping effects, which is a very important supplement for better understanding the VIV of bridge deck. The paper is organized as follows. In Section 2, the experiments of VIV tests of a twin-box girder are described. In Section 3, the experimental results which are concerned about the VIV characteristics of a twin-box girder are discussed in detail, including the VIV responses, aerodynamic forces, flow structures, and damping effects. Finally, conclusions are drawn in Section 4.

2. Experimental setup

The experiments were conducted in a closed-loop wind tunnel (WTWF-HIT, Harbin Institute of Technology, P. R. China), which has a small test section and a large test section, both rectangular. In this study, the experiments were carried out in the small test section with a cross-section of 4 m $\times$ 3 m. The turbulence intensity of the free stream is less than 0.46% over the speed range of 2–50 m/s, and the non-uniformity of free-stream is no stronger than 1%.

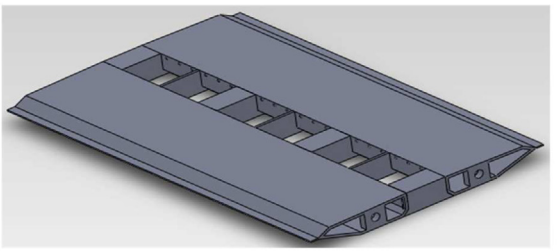

(a)3-D sketch of twin-box girder

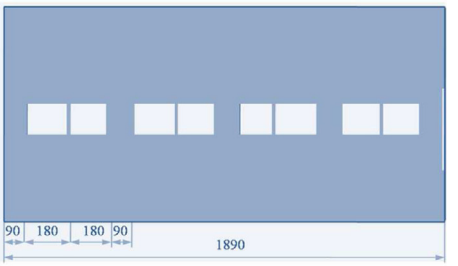

(b)Top view of the section model

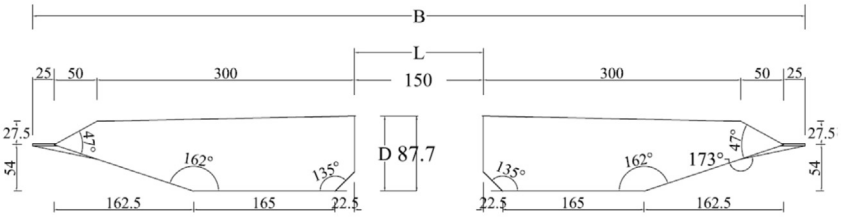

(c) Section view (mm)

Fig. 1. Geometrical dimensions of the section model.

Table 1
Parameters of section model test.

Parameters	Unit	Value of prototype	Similarity ratio	Value of section model
Mass	Kg/m	27 511	λ_m = 1:40^2	16.50
Inertial moment I_m	Kg-m^2/m	4 002 800	λ_{Im} = 1:40^4	1.50
Vertical natural frequency f_h	Hz	0.1831	λ_{fh} = 28.25:1	5.173
Torsional natural frequency f_t	Hz	0.2295	λ_{ft} = 27.80:1	6.381
Vertical damping ratio ξ_h	‰	–	λ_ξ = 1	0.21–1.56
Torsional damping ratio ξ_t	‰	–	λ_ξ = 1	0.23–1.59

In the study, the investigated bridge is Xihoumen Bridge without attachments structures. The geometric scale ratio of the section model is 1:40. The detailed geometrical dimensions of the section model is shown in Fig. 1. The twin-box girder has two parallel box girders with a gap of length L = 150 mm and width B = 900 mm, and the center height of the deck D = 87.7 mm. The total length of the sectional model is 1890 mm.

Fig. 2 presents the experimental apparatus used in dynamic experiments. The sectional model is supported by springs. Therefore, the section model can be allowed to have vertical and torsional motions. Each side has one oil damper which can control the system damping by changing its viscosity. The geometrical blockage ratio of the section model is 2.9%. Hence the blockage effect can be ignored with a small blockage ratio. In addition, each side of the test system has one large endplate and one thin ellipse endplate to eliminate the disturbance of the test system. Table 1 shows the specific dynamic properties of the spring-suspended sectional models.

To better understand the flow characteristics of twin-box girder in VIV motions, the smoke-wire flow visualization system was adopted to capture the instantaneous flow patterns around the twin-box girder. The detailed information about the smoke-wire flow visualization system used in the study can be referred to the publication (Laima and Li, 2015). The smoke-wire flow visualization system can be used in the range of U_∞ = 2–3.65 m/s.

To capture the free stream flow velocity and the frequency of vortex shedding, three one-dimensional hotwire probes (Dantec 55P11) were installed in 1 m upstream from the leading edge of the sectional model, near the downstream surface of the gap and the tail of the downstream girder along the flow direction, respectively. The detailed location information of the probes is shown in Fig. 3. The probes were connected by 54N80 Multichannel (Dantec Dynamics Corp [@]), which could realize 8-channel signal synchronous sampling. In this study, the sampling frequencies of all hotwire probes were set to 1 kHz.

Two laser displacement meters (B&K Corp [@], 4507B) were arranged on the supporting beams to measure vertical accelerations and torsional accelerations, and each of the laser displacement meters was installed 750 mm away from the longitudinal axis of the section model. The sampling frequencies of laser displacement meters were also set to 1 kHz.

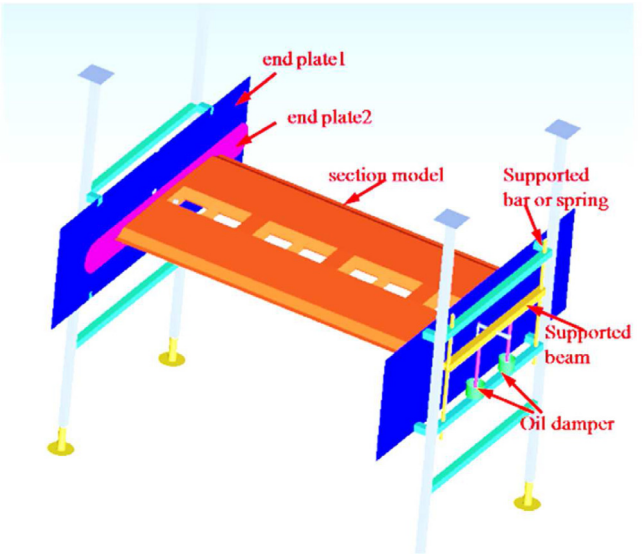

Fig. 2. A sketch of experimental apparatus for dynamic tests.

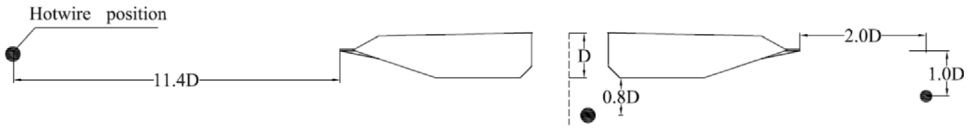

Fig. 3. Locations of hotwire points.

3. Results and discussions

3.1. Characteristic of VIV responses of the twin-box girder

According to Table 1, the natural vertical frequency is $f_n = 5.173$ Hz, the vertical damping ratio is $\xi = 0.21\%$, and the dimensionless mass ($m^* = m/(\rho V)$, m is the mass per unit length, ρ is the air density, V is the volume per unit length) is $m^* = 486.5$. Hence, the Skop–Griffin number can be calculated out $S_G = 1.8714$ (the Skop–Griffin number can be written as $S_G = 2\pi^3 m^* \xi St^2$, which is an important parameter to present the ability of VIV of the buff body). The torsional vibration frequency of the free vibration system is $f_n = 6.381$ Hz, and the critical damping ratio is $\xi = 0.25\%$. The vortex-induced vibration (VIV) test is composed of loading (increasing wind velocity) and unloading (decreasing wind velocity) tests. In the loading test, the free stream flow velocity was gradually loaded from 2 m/s to 3.65 m/s with approximately of about 0.05 m/s increments. Then the unloading test was carried out. The flow velocity was gradually unloaded from 3.65 m/s to 2 m/s in increments of 0.05 m/s. In the experiment, the twin-box girder only has vertical vortex-induced vibration. Fig. 4 shows the time–history of the vertical vibration displacement of the sectional model during the loading process and the corresponding wind velocity.

The relationship between the root mean square (RMS) of VIV displacement and reduced velocity is shown in Fig. 5, and it can be observed that the lock-in region of the VIV of the twin-box girder is $4.680 \leq U_r \leq 6.113$. In the loading test, the displacement increases exponentially in the range of $4.680 \leq U_r \leq 5.638$, and the relationship can be expressed as follow:

$$\frac{\mathrm{RMS}(y)}{D} = 3.22 \times 10^{-8} e^{2.424 U_r} \tag{1}$$

The maximum dimensionless VIV displacement $\mathrm{RMS}(y)/D = 0.03308$ occurs at reduced velocity $U_r = 5.949$. In addition, the strength of VIV begins to weaken at $U_r = 6.113$, surprisingly, the VIV phenomenon disappears, and the VIV displacement attenuates to zero at $U_r = 6.276$. In the vertical VIV displacement increasing region, the amplitude of VIV displacement changes gradually. And it differs considerably from the VIV phenomenon of the bare circular cylinder, which has sudden changes. In unloading tests, there are weak vibrations in the range of $4.680 \leq U_r \leq 5.005$, and the amplitude coincides with the loading test. Comparing the VIV displacement changes during the loading and unloading stages, it can be observed that there exists a hysteresis phenomenon.

As Fig. 6 shows, in the lock-in region, the VIV frequency is very close to the natural frequency of the free vibration system, but it still changes slightly with the reduced wind velocity. The relationship between VIV frequency and reduced

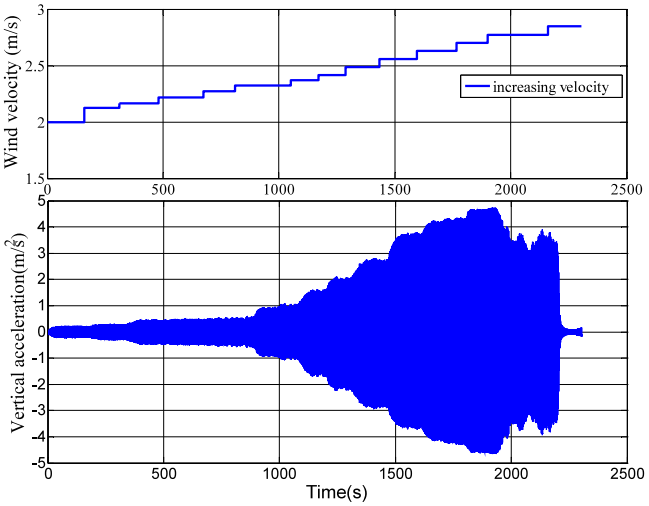

Fig. 4. Time–history of vertical VIV of twin-box girder and corresponding wind velocity at the loading stage.

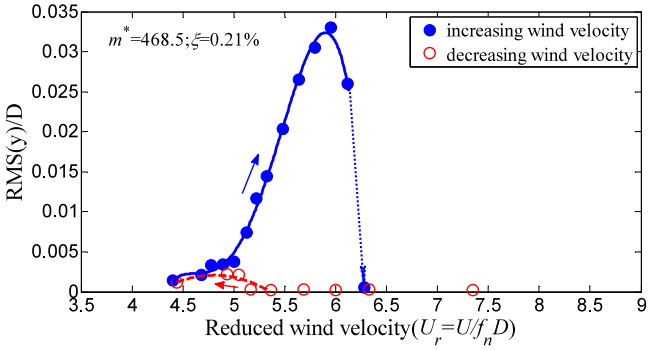

Fig. 5. RMS of vertical VIV of the twin-box girder versus reduced wind velocity.

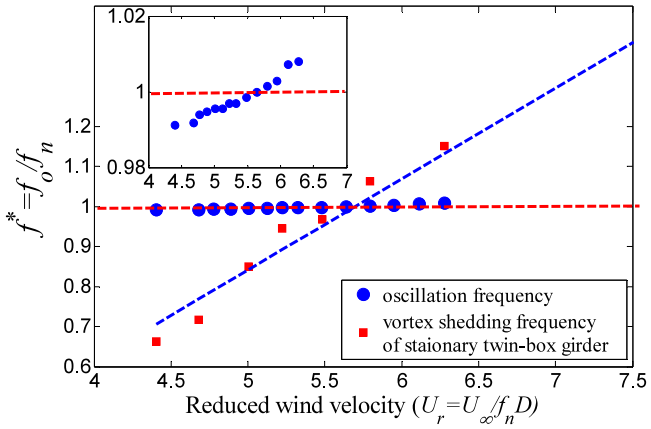

Fig. 6. Oscillation frequency of vertical vortex-induced vibration of twin-box girder versus reduced wind velocity.

wind velocity can be expressed as: the VIV frequency shows an increasing tendency as the reduced velocity increases. The VIV frequency is less than the natural frequency but gradually approaches the natural frequency at $4.680 \leq U_r \leq 5.638$. It indicates that the effect of the aerodynamic force on the negative stiffness of the system continuously weakens. The VIV frequency is higher than the natural frequency and gradually deviates from the natural frequency at $5.638 \leq U_r \leq 6.113$, demonstrating that the effect of the aerodynamic force on the positive stiffness of the system gradually strengthens.

3.2. Characteristics of aerodynamic forces

The frequency and amplitude of aerodynamic force and the phase lag with structural vibration displacement are important VIV parameters. There are three main methods to obtain VIV aerodynamic forces in the wind tunnel tests. First, the aerodynamic forces can be obtained by integrating the surface-pressure. This method is relatively reliable, however, capturing more accurate aerodynamic forces requires a large number of pressure taps, and it might cause the difficulties of synchronous sampling of pressure signals, and displacement signals at each pressure tap is considerable. Second, the aerodynamic forces can be directly measured by force/torque transducers. This measurement demands that the transducers are synchronized with the instantaneous movement of the body, and the damping of the measured section between the force sensors can be accuracy obtained, nevertheless it is difficult to achieve in the real application. Third, the self-induced fluid force can be identified from measured dynamic response, which can overcome the synchronous problem. In the previous published articles, the self-induced fluid force is usually firstly assumed as an empirical equation correlated with dynamic response, then the constant parameters are identified using linear or nonlinear parameter identification method. For instance, Yamada and Ichikawa (1992) obtained the flutter derivatives by the method of Extended Kalman Filtering (EKF) form the coupling free vibration response. Sarker et al. (1992) proposed a Modified Ibrahim Time Domain (MITD) method to identify the linear flutter derivatives from displacement of free vibration. Gu et al. (2000) proposed a Unifying Least Square (ULS) to identify Scanlan linear flutter derivatives form the coupling free vibration response. Li et al. (2003) developed a weighting ensemble least-square method (WELS) to extract all eight flutter derivatives of bridge deck from free vibration records. Ehsan and Scanlan (1990) proposed a nonlinear aerodynamic force model of VIV, which has the form of Van der Pol oscillator, and used decay and growth to steady-state oscillations to identify the parameters according to the first-order approximate solution. Larsen (1995) proposed a generalized nonlinear vortex induced force model, in which the parameters can be identified from the instantaneous vibration signal based on the first-order approximate solution. In the study, we do not used above method. For the one consideration is that, we want to directly obtain the aerodynamic force during VIV, however, the empirical equation should be assumed firstly, which may be not very accuracy. The other consideration is that, the dynamic system of the vertical VIV is very simple, which can be assumed as only having one vertical freedom. If the mass, damping, stiffness of the structure, and the displacement, velocity and acceleration of the vibration system can be accurately obtained, the aerodynamic forces can be calculated from the displacement, velocity, and acceleration of the bridge deck by using the motion equation of a single-degree-of-freedom system. For the mass of the structure, it is very easy to measure, and damping, stiffness of the structure can be identified from free attenuated vibration test in the still air. Moreover, the velocity and acceleration could be obtained by differentiating the displacement once and twice. Therefore, in theory, the self-induced fluid force can be obtained from measured dynamic response directly. However, in practice, due to the influence of the nonlinear factors induced by supporting springs and noise, the free oscillation equation cannot be obtained accurately. Some research works show that the dynamic system of VIVs of twin-box girder is a weakly nonlinear resonance system in which the effect of high-order components is negligible. Therefore, the first-order aerodynamic force component could be obtained by filtering out the high-order components of vertical displacement. The method has been validated in the study of Gharib (1999).

The equation of a single-degree-of-freedom motion under wind force action can be written as follow:

$$m\ddot{y} + c\dot{y} + ky + g(y, \dot{y}) = \frac{1}{2}\rho U^2 C_{\mathrm{L}}(t) B L_e \tag{2}$$

where m represents the mass of the vibration system, namely, twin-box girder; ρ denotes the fluid density; c is the linear damping coefficient; k is the linear stiffness; g is the nonlinear term of the system; $C_L(\mathrm{t})$ is the instantaneous lift force coefficient, y is the vertical displacement of the system, and L_e denotes the length of the sectional model.

Filtering the signals of displacement, velocity, acceleration, and aerodynamic lift force, each term of Eq. (2) can be expressed as:

$$\begin{aligned} y_1(t) &= \int G(r) y(t-r) dr \\ \dot{y}_1(t) &= \int G(r) \dot{y}(t-r) dr \\ \ddot{y}_1(t) &= \int G(r) \ddot{y}(t-r) dr \\ C_{\mathrm{L1}}(t) &= \int G(r) C_{\mathrm{L}}(t-r) dr \end{aligned} \tag{3}$$

where y_1 denotes the signal after filtering; G represents the filtering function.

Assuming that the residuals of the filtered value of displacement, velocity, acceleration, and aerodynamic force from the original signal are y_2, $\dot{y}_2$ $\ddot{y}_2$ and C_{L2}, respectively. Hence the original signal can be expressed as follows:

$$\begin{aligned} y(t) &= y_1(t) + y_2(t) \\ \dot{y}(t) &= \dot{y}_1(t) + \dot{y}_2(t) \\ \ddot{y}(t) &= \ddot{y}_1(t) + \ddot{y}_2(t) \\ C_{\mathrm{L}}(t) &= C_{\mathrm{L1}}(t) + C_{\mathrm{L2}}(t) \end{aligned} \tag{4}$$

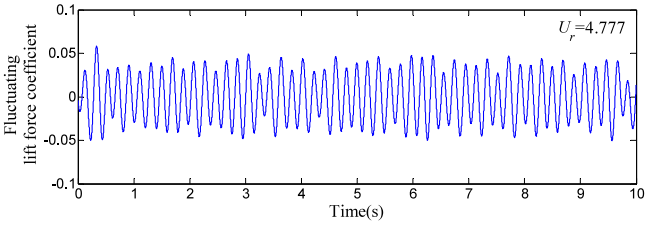

(a)U_r=4.777

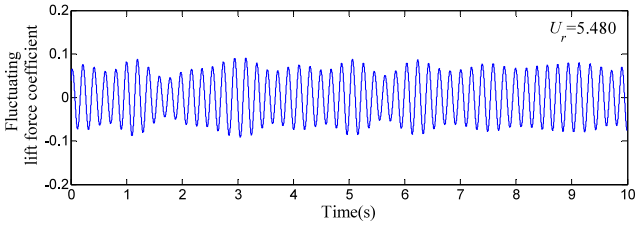

(b)U_r=5.480

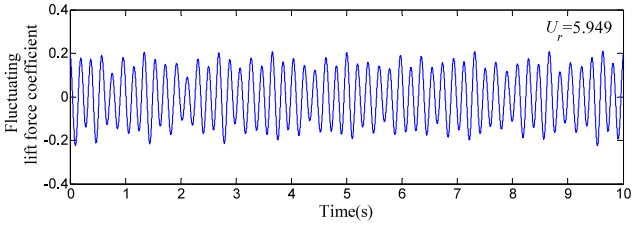

(c)U_r=5.949

Fig. 7. Times histories of lift force of twin-box girder at various reduced wind velocity.

Eqs. (4) into (2), the following equation can be obtained:

$$m\ddot{y}_1 + c\dot{y}_1 + ky_1 + m\ddot{y}_2 + c\dot{y}_2 + ky_2 + g(y_1 + y_2, \dot{y}_1 + \dot{y}_2) = \frac{1}{2}\rho_{air}U^2C_{L1}(t) + \frac{1}{2}\rho U^2C_{L2}(t) \tag{5}$$

To filter out the influence of high-frequency components, band-pass filtering is performed on the vertical vibration signal of vortex-induced vibration in the frequency range $1/2f_n < f < 2f_n$. Assuming that the nonlinear term $g(y_1 + y_2, \dot{y}_1 + \dot{y}_2)$ does not produce frequency components containing f_n, the first-order aerodynamic lift force component of Eq. (4) can be written as follow:

$$m\ddot{y}_1 + c\dot{y}_1 + ky_1 = \frac{1}{2}\rho U^2C_{L1}(t) \tag{6}$$

Fig. 7 shows that the time–history of fluctuating lift force coefficient, at $U_r = 4.777$, $U_r = 5.480$ and $U_r = 5.949$ respectively. Substituting the instantaneous fluctuating lift force coefficient into Eq. (6), the dimensionless displacement only with the effect of the first-order aerodynamic lift force component can be obtained by adopting the Newmark-β method. Fig. 8 compares the time–history of the dimensionless displacement calculated by Eq. (6) with the experimental results, and the calculated results are consistent with the measured results. Fig. 8 demonstrates that the dynamic response of VIV is mainly determined by the first-order aerodynamic component.

As VIV entering the lock-in range, the fluid–structure interaction gradually strengthens and the interaction between aerodynamic lift force and system vibration appears. The relationship between the RMS of aerodynamic lift force coefficient and the reduced wind velocity, the interrelation between the RMS of VIV displacement and the aerodynamic lift force coefficient, and the interconnection between the phase and the reduced flow velocity are shown in Figs. 9, 10, and 11, respectively. It can be seen from Figs. 9, 10, and 11 that the change of VIV aerodynamic lift force is comprised of 5 stages. In stage 1, the amplitude of aerodynamic lift force does not vary with the reduced wind velocity, meanwhile,

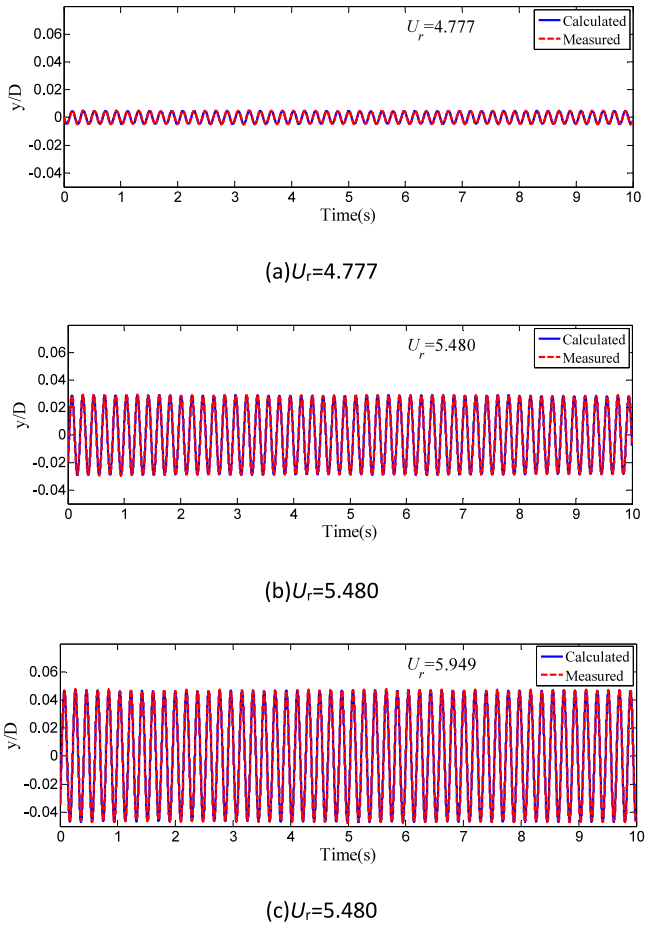

Fig. 8. Times histories of measured VIV displacement and calculated displacement based on first order aerodynamic lift force.

the phase lag and the amplitude of VIV displacement gradually increases with the increasing of reduced velocity. In stage 2, the amplitude of the aerodynamic lift force shows a slightly decreasing tendency, however, it is larger than the value of stage 1. The phase lag gradually rises to 90 degrees which means that the aerodynamic lift force and flow velocity are in the same direction and the amplitude of VIV displacement continuously increases, as the reduced velocity increases. In stage 3, the amplitude of the aerodynamic lift force significantly increases and the amplitude of VIV displacement keeps increasing. Conversely, the phase lag gradually turns 90 degrees to 180 degrees which denotes that the direction of the aerodynamic lift force is opposite to the VIV displacement. In stage 4, the aerodynamic lift force rises to its maximum value, the phase lag is 165 degrees, and the amplitude of VIV displacement begins to decrease. In stage 5, the aerodynamic force is almost zero, the phase lag is 172 degrees, and the VIV phenomenon of twin-box girder disappears. In the region of VIV, the phase lag of VIV displacement and the aerodynamic force changes continuously without a sudden break. As the aerodynamic lift force increases, both the phase lag and the VIV displacement show an increasing tendency with the reduced velocity, and the relationship between phase lag and reduced wind velocity can be expressed as follow:

$$\theta = 2.07 \times 10^{-4} e^{2.315 U_r} \tag{7}$$

When the VIV motion of twin-box girder is stable, the VIV displacement can be written as:

$$y = A \sin(2\pi f t) \tag{8}$$

where A represents the amplitude of VIV displacement and f denotes the VIV frequency.

Assuming the phase lag between the VIV displacement and the aerodynamic lift force is θ, hence the instantaneous aerodynamic lift force coefficient can be expressed as:

$$C_L(t) = C_{L0} \sin(2\pi f t + \theta) \tag{9}$$

where C_{L0} denotes the amplitude of the aerodynamic lift force coefficient.

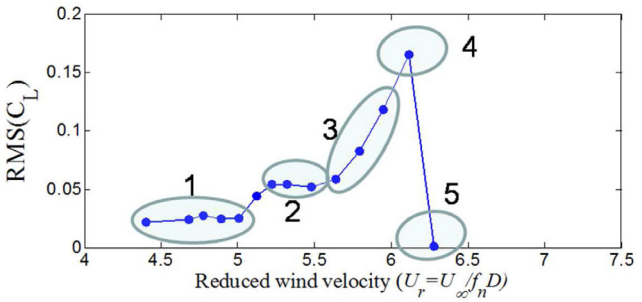

Fig. 9. RMS of fluctuating lift-force vs. Reduced wind velocity.

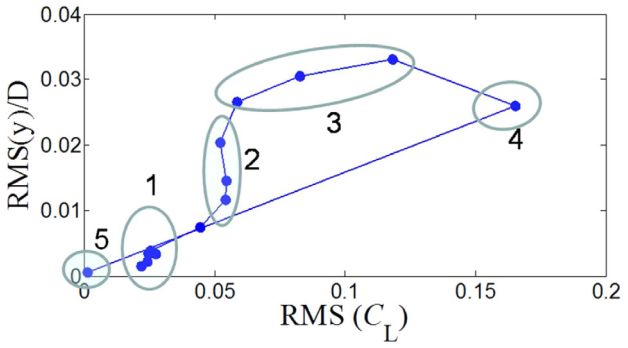

Fig. 10. Relationship between RMS of oscillation displacement and RMS of fluctuating lift-force.

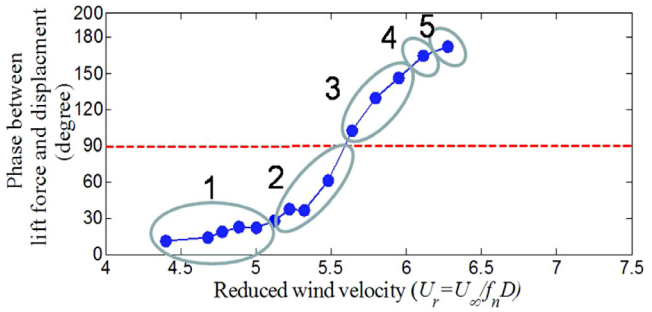

Fig. 11. Phase between lift force and vertical displacement versus reduced velocity.

Eq. (9) can be rewritten as follow:

$$C_L(t) = (C_{L0}\cos\theta)\sin(2\pi ft) + (C_{L0}\sin\theta)\cos(2\pi ft) \tag{10}$$

It can be found that the first term has the same phase lag with the VIV displacement, in other words, the first term denotes the aerodynamic stiffness coefficient. The second term has the same phase lag with the vibration velocity of the VIV motions, namely, the second term represents the aerodynamic damping coefficient.

The relationship between the RMS of VIV displacement, the RMS of the aerodynamic damping force, and the RMS aerodynamic resilience force are shown in Fig. 12(a) and (b). Moreover, Fig. 12(a) also presents the interconnection between the amplitude of VIV displacement and the structural damping force. As VIV motion entering the stable stage, the aerodynamic damping, and structural damping cancel each other. However, it can be seen from Fig. 12(a) that the aerodynamic damping is slightly larger than the structural damping in the ascending section, indicating that the calculated aerodynamic damping is not completely accurate. In the calculation of aerodynamic damping force, the average phase angle calculated by aerodynamic lift and displacement is used. However, for a weakly nonlinear system, the phase of aerodynamic damping and displacement is a time variable. In addition, the relationship between aerodynamic damping and structural displacement is not a simple linear relationship in the rising stage of vortex-induced vibration, and the aerodynamic damping in the descending section is also different from that in the ascending stage. For the relationship

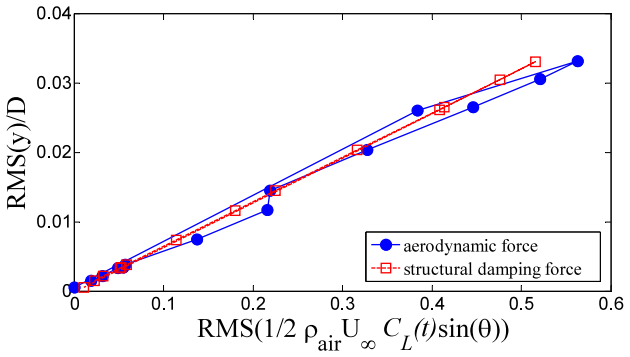

(a) Aerodynamic damping force

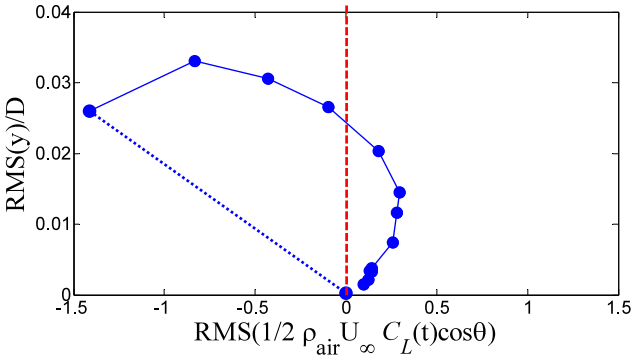

(b) Aerodynamic resilience force

Fig. 12. Aerodynamic lift force versus reduced wind velocity.

between aerodynamic resilience force and vibration displacement, as shown in Fig. 12(b), the aerodynamic stiffness of vortex-induced vibration changes from one stable stage to another.

3.3. Characteristics of the flow pattern of VIV motion around the twin-box girder

Fig. 13 presents the flow field structure around the box girder. For the stationary case (see Fig. 13(a)), the flows separate at the leading edges on the upper and lower surfaces of the upstream box girder. Due to the Kelvin–Helmholtz instability of the separation boundary layer, vortices shed from the upper and lower separated shear layer, and propagates downstream and merge with the trailing vortices, producing alternately shedding vortex in the wake. It should be noted that the upper and lower shear layers do not interact with each other around the gap. Due to the streamline aerodynamic design, the separation of flow on the surface of the box girder and strength of the shedding vortex is relatively weak.

Compared with the stationary case, the most significant change of the flow pattern of the VIV of the twin box girder is that the alternately shedding vortices appear around the gap, as shown in Fig. 13(b) and (c). With the increase of the amplitude of vortex-induced vibration, the alternately shedding vortex becomes stronger. Under the influence of the vortex generated in the gap, the size of the separation bubble increases with the increase of vibration amplitude, and the wake width becomes wider, and the flow state around the downstream box girder is gradually controlled by the vortex in the gap.

When the VIV enters the lock-in region, the vortex shedding process is controlled by the structural vibration due to the interaction between fluid and structure vibration. Fig. 14 shows the variation of structural vibration frequency, vortex shedding frequency, and vortex-induced aerodynamic frequency with reduced wind speed. The vortex-shedding frequency can be obtained by the power spectra of velocities around the gap and the wake of the downstream box girder. As shown in the figure, the dominant frequencies of oscillation, vortex shedding, and lift force are close to the natural frequency of the body, but it should be noted there still are differences among the three frequencies. For the structural oscillation frequency, it increases continuously with the increase of reduced wind speed. However, for the vortex shedding frequency and the aerodynamic dominant frequency, they display stepped variation. As the figure shows, in $4.680 \leq U_r \leq$

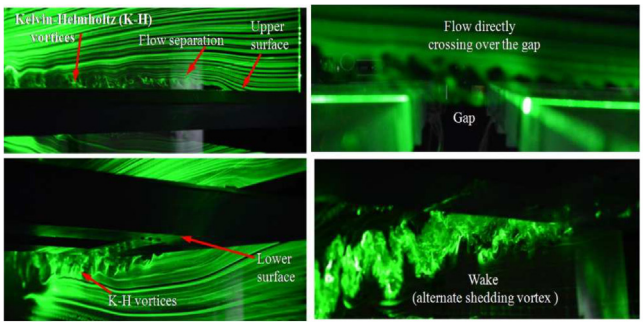

(a) Stationary case

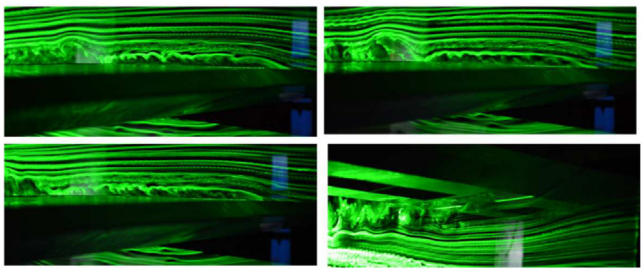

(b) U_r=5.223, initial stage of VIV

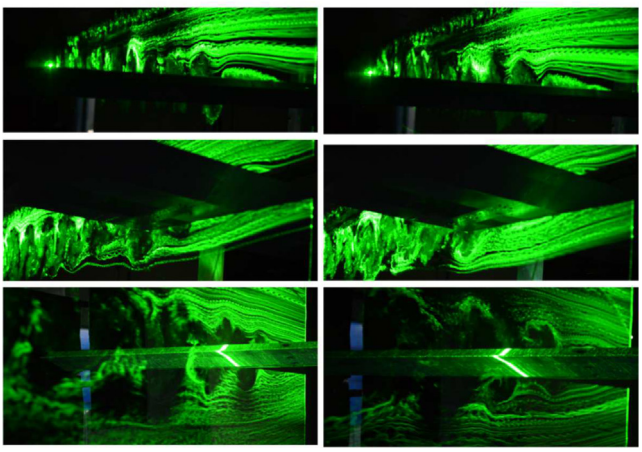

(c) U_r=5.949, in the stage with the largest amplitude of VIV

Fig. 13. Flow visualization around the twin-box girder.

5.223, the vortex shedding process is not completely controlled by vibration. Except for the components close to the structural vibration frequency, there are other vortex shedding frequency components in the fluid. While in the range of $5.223 < U_r \leq 6.113$, the vortex shedding process is completely controlled by vibration, and the shedding frequency is almost equal to the structural vibration frequency.

Fig. 14 also shows the variation of vortex shedding frequency with wind speed for the stationary twin-box girder. According to the definition of the VIV of the body, it is generally believed that the vortex shedding frequency of fluid at the tail of the structure is close to the natural frequency of the structure as the VIV appears. However, it can be found from the figure that, the dimensionless vortex shedding of the stationary box girder (f_v/f_n) is only 0.6629 at critical $Ur = 4.80$, which is far less than 1. For the streamlined twin-box girder, although the velocity fluctuation caused by vortex shedding has a dominant frequency, the energy is not concentrated and shows a broadband characteristic when the vortex-induced vibration does not occur. When the natural frequency of the structure locates in the broadband range and the energy is large enough, the vortex-induced vibration can be excited. Some vortices are controlled by vibration

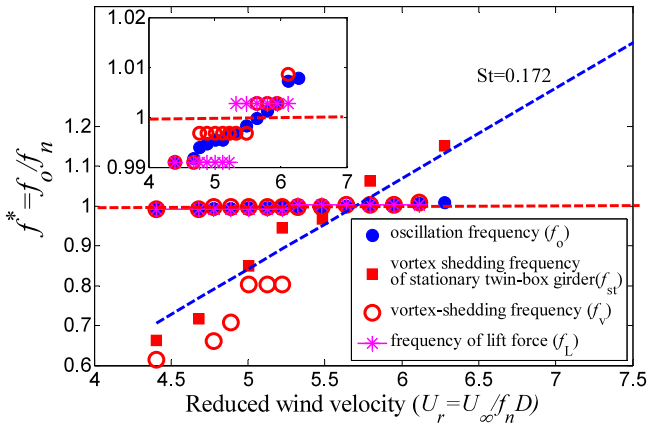

Fig. 14. Vortex shedding frequency of twin box girder during VIV occurring versus reduced wind velocity.

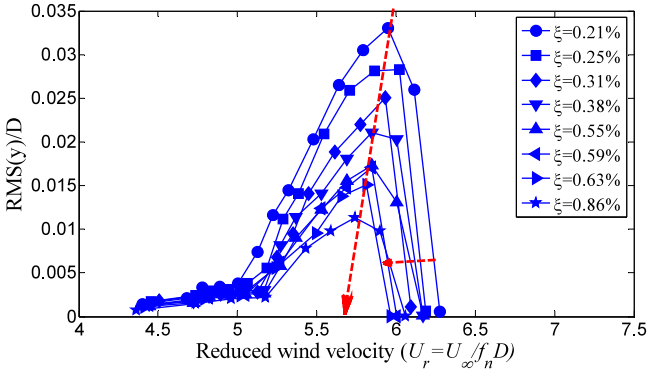

Fig. 15. RMS of vertical VIV of twin-box girder versus reduced wind velocity at various damping ratios.

due to the coupling between structure vibration and the surrounding fluid. However, due to the weak coupling effect, some vortices with larger energy still maintain their original frequency. When the vibration amplitude begins to increase, the vortex shedding around the box girder is completely locked by the structural vibration.

3.4. The effect of damping on vortex-induced vibration of the twin box girder

The RMS of VIV displacement versus the reduced wind velocity at various damping ratios is shown in Fig. 15. It can be found that the damping ratio is a significant factor to control the VIV motion, and the amplitude of VIV displacement shows a decreasing tendency, the lock-in region becomes narrower and the reduced velocity corresponding to the max VIV displacement decreases as the damping ratio increases. Under constant mass ratio, the maximum RMS displacement of vertical VIV decays exponentially as the damping ratio increases, as shown in Fig. 16. And the function between the maximum RMS displacement of vertical VIV and damping ratio can be written as follow:

$$\frac{RMS(y)}{D} = 0.04138e^{-151.5\xi} \tag{11}$$

Fig. 17 compares the relationship between the maximum RMS displacement of vertical VIV and Skop–Griffin parameter (S_G) with that of the circular cylinder, the relationships can be expressed as follows:

$$\begin{aligned}\frac{RMS(y)_{twin-box-girder}}{D} &= 0.04413e^{-0.2105S_G}\\ \frac{RMS(y)_{circular-cylinder}}{D} &= 0.7918e^{-1.050S_G}\end{aligned} \tag{12}$$

Owing to the considerable differences in aerodynamic configurations, the flow characteristics of the twin-box girder differ significantly from that of the bare cylinder. For bare circular cylinders, the flow separates from the surface and then generates strong vortex-shedding at the wake forming Karman vortex. For streamlined box girders, the boundary layer not only separates at the tail with alternative vortex-shedding but also generates complex flow separation and reattachment phenomena at the leading edge. In addition, more complicated flow structures might be generated around the gap. Due

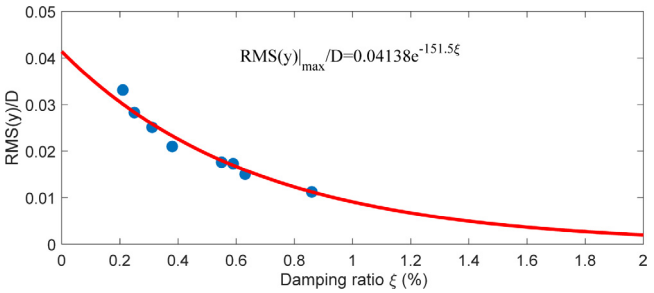

Fig. 16. Maximum RMS displacement of vertical VIV of twin-box girder as a function of damping ratio.

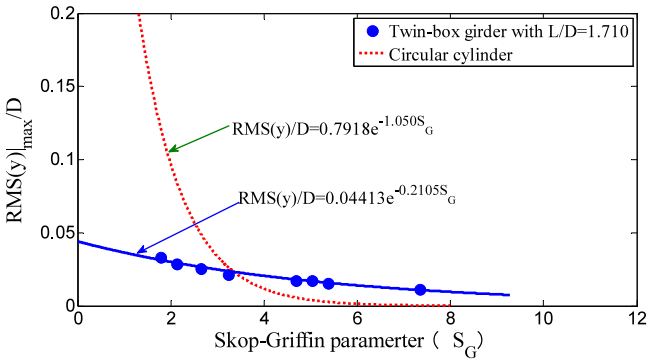

Fig. 17. Maximum RMS displacement of vertical VIV of twin-box girder as a function of S_G parameter.

to the significant difference in the flow structures, there are huge differentiation in the characteristics of VIVs between twin-box girder and bare cylinder.

Compared with the regular pattern of a circular cylinder, it can be observed that at $S_G < 3.5$, the amplitude of RMS displacement of vertical VIV is much smaller than that of rigid cylinders. For instance, the maximum RMS dimensionless-displacement of vertical VIV (RMS(y)/D) is 0.0468 and that of circular cylinders is 0.1556 at the same Skop–Griffin parameter of $S_G = 1.875$. Fig. 16 also shows that the attenuation of maximum VIV displacement of the twin-box girder with S_G is slower than that of circular cylinders. For example, at $S_G > 3.5$, the maximum VIV vertical displacement of the twin-box girder is larger than that of the cylinders.

Moreover, the phase difference between lift force and displacement of vertical VIV of twin-box girder continuously changes throughout the entire vortex-induced vibration process without phase jump. While the phase jump is a significant phenomenon in the VIV of cylinders, because it represents vortex-shedding pattern switching (Williamson and Govardhan, 2004).

Last but not least, in the VIV of cylinders, there are three branches, namely initial branch, upper branch, and lower branch, in the vertical displacement, while the vertical displacement of VIV of twin-box girder has no obvious branches. The amplitude of vertical displacement of twin-box girder changes continuously during the ascending phase, and after a very short descending period, it suddenly decays to zero. Although the hysteresis exists in the VIV of the twin-box girder, the amplitude of vertical displacement is limited in the unloading stage.

4. Conclusions

In this study, the investigations of vortex-induced vibrations of twin-box girder are executed. And the characteristics of VIV response of bridge deck, the characteristics of aerodynamic force, and the damping effects on the VIV have been analyzed in detail. The conclusions are summarized as follow:

(1) For the approximate streamline box girder with large aspect ratio, the VIV amplitude is much smaller than that of the bluff body in low S_G number, however, the VIV amplitude is much larger than that of bluff body in high S_G number.
(2) For the bluff body, there usually have three branches, namely initial branch, upper branch, and lower branch, in the vertical displacement, while the vertical VIV of approximate streamline box girder has no obvious branches. The amplitude of vertical displacement of twin-box girder changes continuously during the ascending phase, and after a very short descending period, it suddenly decays to zero.

(3) The phase difference between lift force and displacement of vertical VIV of the approximate streamline box girder continuously changes throughout the entire vortex-induced vibration process form 0 degree to 180 degree without phase jump, which implies that there is not vortex-shedding pattern switching during the VIV.
(4) The structural damping has significant effects on the development of VIV of approximate streamline box girder. As the damping ratio increases, the amplitude of VIV displacement shows a decreasing tendency, the lock-in region becomes narrower and the reduced velocity corresponding to the max VIV displacement decreases. Moreover, the maximum RMS displacement of vertical VIV decays exponentially as the damping ratio increases.

CRediT authorship contribution statement

Buchen Wu: Validation, Formal analysis, Investigation, Data curation, Writing - review & editing, Visualization. **Shujin Laima:** Conceptualization, Methodology, Software, Validation, Formal analysis, Investigation, Resources, Writing - original draft, Writing - review & editing, Visualization, Supervision, Project administration, Funding acquisition.

Declaration of competing interest

The authors declare that they have no known competing financial interests or personal relationships that could have appeared to influence the work reported in this paper.

Acknowledgments

This study is financially supported by the NSFC, China under Grant Nos. 51878230 and supported by Fundamental Research Funds for the Central Universities, China.

References

Brika, D., Laneville, A., 1993. Vortex-induced vibrations of a long flexible circular cylinder. J. Fluid Mech. 250, 481–481.
Diana, G., Resta, F., Belloli, M., Rocchi, D., 2006. On the vortex shedding forcing on suspension bridge deck. J. Wind Eng. Ind. Aerodyn. 94 (5), 341–363.
Ehsan, F., Scanlan, R.H., 1990. Vortex-induced vibrations of flexible bridges. J. Eng. Mech. 116 (6), 1392–1411.
Feng, C.C., 1968. The Measurement of Vortex Induced Effects in Flow Past Stationary and Oscillating Circular and D-Section Cylinders (Doctoral dissertation). University of British Columbia.
Frandsen, J.B., 2001. Simultaneous pressures and accelerations measured full-scale on the Great Belt East suspension bridge. J. Wind Eng. Ind. Aerodyn. 89 (1), 95–129.
Fujino, Y., Yoshida, Y., 2002. Wind-induced vibration and control of Trans-Tokyo Bay crossing bridge. J. Struct. Eng. 128 (8), 1012–1025.
Gao, G., Zhu, L., 2015. Nonlinearity of mechanical damping and stiffness of a spring-suspended sectional model system for wind tunnel tests. J. Sound Vib. 355, 369–391.
Gao, G., Zhu, L., Han, W., Li, J., 2018. Nonlinear post-flutter behavior and self-excited force model of a twin-side-girder bridge deck. J. Wind Eng. Ind. Aerodyn. 177, 227–241.
Ge, Y.J., Yang, Y.X., Cao, F.C., 2011. VIV sectional model testing and field measurement of Xihoumen Suspension Bridge with twin box girder. In: Proceedings of the 13th International Conference on Wind Engineering, Amsterdam, Netherlands, July, pp. 11–15.
Gharib, M.R., 1999. Vortex-Induced Vibration, Absence of Lock-in and Fluid Force Deduction (Ph.D. thesis). California Institute of Technology.
Gu, M., Zhang, R., Xiang, H., 2000. Identification of flutter and bridge deck. J. Wind Eng. Ind. Aerodyn. 84 (2), 151–162.
Klamo, J.T., Leonard, A., Roshko, A., 2005. On the maximum amplitude for a freely vibrating cylinder in cross-flow. J. Fluids Struct. 21 (4), 429–434.
Laima, S., Li, H., 2015. Effects of gap width on flow motions around twin-box girders and vortex-induced vibrations. J. Wind Eng. Ind. Aerodyn. 139, 37–49.
Laima, S., Li, H., Chen, W., Li, F., 2013. Investigation and control of vortex-induced vibration of twin box girders. J. Fluids Struct. 39, 205–221.
Laima, S., Li, H., Chen, W., Ou, J., 2018. Effects of attachments on aerodynamic characteristics and vortex-induced vibration of twin-box girder. J. Fluids Struct. 77, 115–133.
Larsen, A., 1995. A generalized model for assessment of vortex-induced vibrations of flexible structures. J. Wind Eng. Ind. Aerodyn. 57 (2), 281–294.
Larsen, A., Esdahl, S., Andersen, J.E., Vejrum, T., 2000. Storebælt suspension bridge–vortex shedding excitation and mitigation by guide vanes. J. Wind Eng. Ind. Aerodyn. 88 (2–3), 283–296.
Larsen, A., Savage, M., Lafrenière, A., Hui, M.C., Larsen, S.V., 2008. Investigation of vortex response of a twin box bridge section at high and low Reynolds numbers. J. Wind Eng. Ind. Aerodyn. 66, 476–489.
Li, L.Y., Ge, Y.J., 2008. Experiments of vortex control for central-slotting on long-span bridges. J. Huazhong Univ. Sci. Technol. 36 (12), 112–115.
Li, H., Laima, S., Jing, H., 2014. Reynolds number effects on aerodynamic characteristics and vortex-induced vibration of a twin-box girder. J. Fluids Struct. 50, 358–375.
Li, H., Laima, S., Ou, J., et al., 2011. Investigation of vortex-induced vibration of a suspension bridge with two separated steel box girders based on field measurements. Eng. Struct. 33 (6), 1894–1907.
Li, Y., Liao, H., Qiang, S., 2003. Weighting ensemble least-square method for flutter derivatives of bridge decks. J. Wind Eng. Ind. Aerodyn. 91 (6), 713–721.
Li, Z., Zhou, Q., Liao, H., Ma, C., 2018. Numerical studies of the suppression of vortex-induced vibrations of twin box girders by central grids. Wind Struct. 26 (5), 305–315.
Ma, C.M., Wang, J.X., Li, Q.S., Qin, H., Liao, H.L., 2018. Vortex-induced vibration performance and suppression mechanism for a long suspension bridge with wide twin-box girder. J. Struct. Eng. 144 (11), 04018202.
Sarker, P.P., Jones, N.P., Scanlan, R.H., 1992. System identification of aeroelastic parameters of flexible bridges. J. Wind Eng. Ind. Aerodyn. 41–44, 1243–1254.
Williamson, C.H.K., Govardhan, R., 2004. Vortex-induced vibrations. Annu. Rev. Fluid Mech. 36, 413–455.
Williamson, C.H., Roshko, A., 1988. Vortex formation in the wake of an oscillating cylinder. J. Fluids Struct. 2 (4), 355–381.
Yamada, H., Ichikawa, H., 1992. Measurement of aerodynamics coefficients by extended Kalman filter algorithm. J. Wind Eng. Ind. Aerodyn. 42, 1255–1263.
Yang, Y., Zhou, R., Ge, Y., Zhang, L., 2016. Experimental studies on VIV performance and countermeasures for twin-box girder bridge with various slot width ratios. J. Wind Eng. Ind. Aerodyn. 96 (6–7), 934–944.
Zhou, R., Yang, Y., Ge, Y., Zhang, L., 2018. Comprehensive evaluation of aerodynamic performance of twin-box girder bridges with vertical stabilizers. J. Wind Eng. Ind. Aerodyn. 175, 317–327.